Analysis of Cylindrical Cavity Expansion in Modified Cam Clay with *Ko* Consolidation

Vincenzo Silvestri[1(✉)] and Claudette Tabib[2]

[1] École Polytechnique, Montreal, Canada
vincenzo.silvestri@polymtl.ca
[2] Montreal, Canada
claudette.tabib@yahoo.ca

Abstract. This paper presents explicit expressions for the principal effective stresses generated around a cylindrical cavity expanded in plane strain and undrained conditions in Modified Cam Clay. The assumption made in the present analysis is that Poisson's ratio v' remains constant throughout the shearing process. Theoretical expressions are applied to the simulation of a cylindrical cavity expansion test in K_o normally consolidated remoulded Boston Blue Clay modelled as Modified Cam Clay. The results, which are compared to those obtained by assuming that the shear modulus G' remains constant, show that the two approaches are quite similar.

1 Introduction

Chen and Abousleiman (2012) and Silvestri and Abou-Samra (2012) recently obtained semi-analytical solutions for the plane strain undrained expansion of cylindrical cavities in Modified Cam Clay. Chen and Abousleiman (2012) employed small strains, but Silvestri and Abou-Samra (2012) used finite natural strains in both the elastic and plastic phases of the expansion. The latter authors also considered Almansi strains for obtaining the limiting radial expansion pressure. In addition, Silvestri and Abou-Samra (2012) adopted the restrictive assumption that the hardening parameter p'_c, which controls the size of the yield loci, remained constant during shearing. Such simplifying assumption permitted the determination of explicit expressions for the principal effective stresses generated in the soil around the cavity, but it led to approximate responses.

Silvestri and Abou-Samra (2012) also assumed the shear modulus G' to remain constant throughout the expansion process, following the approach of Randolph et al. (1979). From a theoretical point of view, it is preferable to assume a constant shear modulus G', as Zytynski et al. (1978) showed that the use of a constant Poisson's ratio v' would lead to a non-conservative model in the sense that it may not conserve energy during closed-stress cycles (Yu 2006). However, this effect was not important in the case treated by Silvestri and Abou-Samra (2012) since there were no unloading-reloading cycles. As for Chen and Abousleiman (2012), these authors assumed Poisson's ratio v' to remain constant and obtained semi analytical expressions for the principal effective stresses.

W. Frikha et al. (eds.), *Soil Testing, Soil Stability and Ground Improvement*,
Sustainable Civil Infrastructures, DOI 10.1007/978-3-319-61902-6_23

Cao et al. (2001) also obtained an approximate closed-form solution of the undrained cavity expansion in Modified Cam Clay by combining a large strain theory in the plastic zone and a small strain theory in the elastic zone. In the present paper, as the soil is modelled as a non-linear elastic plastic material, elastic and plastic zones are not treated separately. Thus, the analysis cannot be compared directly with Cao et al.'s approach.

In the present paper, both the shear modulus G' and the hardening parameter p'_c vary during undrained shearing, but that Poisson's ratio ν' remains constant. Indeed, Gens and Potts (1988) pointed out that a constant shear modulus did not agree well with experimental measurements and might imply negative values of Poisson's ratio at low stresses, which is physical unreasonable (Yu 2006).

As Poisson's ratio ν' remains constant, such approach allows obtaining explicit expressions for the principal effective stresses generated in the soil around the expanding cylindrical cavity. However, both the total radial pressure and the natural shear strain in the horizontal plane must still be determined numerically. The results obtained in the present paper are applied first to a well-known benchmark case and are thereafter compared with those found by assuming that the shear modulus G' remains constant during the expansion, but that the hardening parameter varies during shearing.

The results also show that the vertical effective stress, which represents the major principal stress at the beginning of the expansion, becomes the intermediate principal stress during the latter stages of the expansion. Similarly, while one of the horizontal effective stresses (i.e., the radial stress) becomes the major principal stress, the other horizontal effective stress (i.e., the tangential stress) becomes the minor principal stress during the expansion. Thus, failure occurs on vertical planes. Such response is different from the one analysed by Monnet (2007). Indeed, this author found that failure in a cylindrical cavity expansion could also occur on inclined planes with the vertical and tangential stresses being the major and minor principal stresses, respectively. Such situation typically arises in expansion tests carried out at shallow depth.

2 Approach

2.1 Modified Cam Clay Model

The general effective stress invariants used in the Modified Cam Clay model are the mean effective stress p' and the deviator stress q, which are defined as:

$$p' = \frac{\sigma'_r + \sigma'_\theta + \sigma'_z}{3} \tag{1a}$$

and

$$q = \left[\frac{\left(\sigma'_r - \sigma'_\theta\right)^2 + \left(\sigma'_\theta - \sigma'_z\right)^2 + \left(\sigma'_z - \sigma'_r\right)^2}{2}\right]^{1/2} \tag{1b}$$

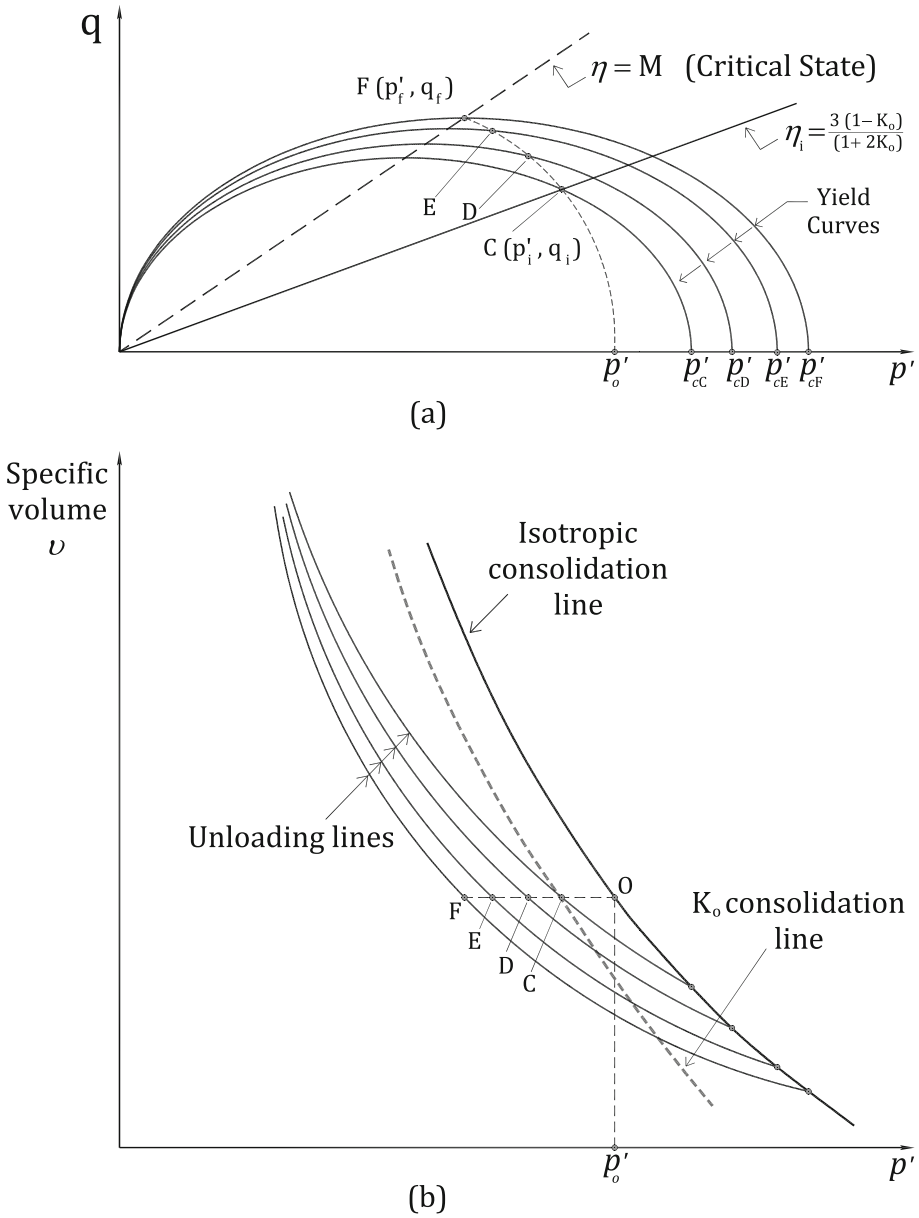

Fig. 1. Undrained compression test on normally consolidated clay: (a) $p' : q$ plane; (b) $\upsilon : p'$ plane (adapted from Wood (2007))

where $\sigma'_r, \sigma'_\theta, \sigma'_z$ = principal radial, tangential, and axial effective stresses. Figure 1a presents various yield curves of the Modified Cam Clay model. Each curve is described by the following expression:

$$q = p'M\left[\left(p'_c/p'\right) - 1\right]^{1/2} \tag{2}$$

where $M = q/p'$ at critical state $= 6sin\phi'/(3 - sin\phi')$, with $\phi' =$ friction angle and $p'_c =$ hardening parameter. The latter parameter controls the size of the yield locus. An effective stress path (ESP) followed by a K_o normally consolidated specimen in an undrained compression test is also reported in Fig. 1a. The ESP is described by the expression

$$q = p'\left[\left(M^2 + \eta_i^2\right)\left(p'_i/p'\right)^{1/\Lambda} - M^2\right]^{1/2} \tag{3a}$$

where

$\eta_i = q_i/p'_i = 3(1 - K_o)/(1 + 2K_o)$,
$q_i = \sigma'_{zi} - \sigma'_{ri} = \sigma'_{zi} - \sigma'_{\theta i} = (1 - K_o)\sigma'_{zi}$,
$p'_i = \left(\sigma'_{ri} + \sigma'_{\theta i} + \sigma'_{zi}\right)/3 = (1 + 2K_o)\sigma'_{zi}/3$,
$\sigma'_{ri} = \sigma'_{\theta i}, \sigma'_{zi} =$ initial horizontal and vertical effective stresses, respectively,
$K_o = \sigma'_{ri}/\sigma'_{zi} = \sigma'_{\theta i}/\sigma'_{zi} =$ in situ coefficient of lateral earth pressure at rest,
$\Lambda = (\lambda - \kappa)/\lambda$,
$\lambda =$ slope of $\upsilon : ln\, p'$ line in loading (Fig. 1b),
$\kappa =$ slope of $\upsilon : ln\, p'$ line in unloading (Fig. 1b),
$\upsilon = 1 + e =$ specific volume, and
$e =$ void ratio.

The ESP may also be described by the following equation:

$$q = p'M\left[\left(p'_o/p'\right)^{1/\Lambda} - 1\right]^{1/2} \tag{3b}$$

where $p'_o =$ value of p' for $q = 0$, as shown in Fig. 1a. The ESP of the K_o normally consolidated specimen begins at point C $\left(p'_i, q_i\right)$ and ends at point F $\left(p'_f, q_f\right)$ on the critical state line, whose coordinates are $p'_f = 2^{-\Lambda}p'_o$ and $q_f = Mp'_f = 2^{-\Lambda}Mp'_o$ (Wood 2007). The undrained shear strength S_u is equal to $q_f/\sqrt{3}$. As the expansion occurs under undrained conditions, the specific volume υ remains constant along the ESP, as shown in Fig. 1b, and each point on the stress path lies on a new yield locus. The test thus moves across progressive higher yield loci, which are associated with expansion of the yield locus and with decrease of the mean effective stress p' for the normally consolidated specimen.

2.2 Modified Cam Clay Stress-Strain Relationships

Silvestri and Abou-Samra (2012) showed that the incremental elastic-plastic relationships of the Modified Cam Clay model in undrained shearing are given by:

$$d\sigma_r' = 2G'd\varepsilon_r + dp'\left[1 + \frac{6G'\kappa\left(\sigma_r' - p'\right)}{\upsilon M^2 p'\left(2p' - p_c'\right)}\right] \tag{4a}$$

$$d\sigma_\theta' = 2G'd\varepsilon_\theta + dp'\left[1 + \frac{6G'\kappa\left(\sigma_\theta' - p'\right)}{\upsilon M^2 p'\left(2p' - p_c'\right)}\right] \tag{4b}$$

$$d\sigma_z' = 2G'd\varepsilon_z + dp'\left[1 + \frac{6G'\kappa\left(\sigma_z' - p'\right)}{\upsilon M^2 p'\left(2p' - p_c'\right)}\right] \tag{4c}$$

where $d\varepsilon_r, d\varepsilon_\theta, d\varepsilon_z$ = incremental radial, tangential, and axial natural strains. However, as $d\varepsilon_z = 0$ in plane strain and $d\varepsilon_r + d\varepsilon_\theta = 0$ in undrained shearing, then Eqs. 4a–4c become:

$$d\sigma_r' = -2G'd\varepsilon_\theta + dp'\left[1 + \frac{6G'\kappa\left(\sigma_r' - p'\right)}{\upsilon M^2 p'\left(2p' - p_c'\right)}\right] \tag{5a}$$

$$d\sigma_\theta' = 2G'd\varepsilon_\theta + dp'\left[1 + \frac{6G'\kappa\left(\sigma_\theta' - p'\right)}{\upsilon M^2 p'\left(2p' - p_c'\right)}\right] \tag{5b}$$

$$d\sigma_z' = dp'\left[1 + \frac{6G'\kappa\left(\sigma_z' - p'\right)}{\upsilon M^2 p'\left(2p' - p_c'\right)}\right] \tag{5c}$$

The shear modulus G' and the hardening parameter p_c' are given by (See, for example, Wood 2007):

$$G' = \frac{3}{2}\frac{(1-2\nu')}{(1+\nu')}\mathrm{K} = \frac{3}{2}\frac{(1-2\nu')}{(1+\nu')}\frac{\upsilon p'}{\kappa} \tag{6}$$

and

$$p_c' = p'\left(p_o'/p'\right)^{1/\Lambda} \tag{7}$$

where ν' = Poisson's ratio and $K = \upsilon p'/\kappa$ = bulk modulus. According to Eq. 6, the shear modulus G' increases as the mean effective stress p' increases. Substitution of G' and p_c' in Eqs. 5a–5c yields:

$$d\sigma'_r = -3\frac{(1-2\nu')}{(1+\nu')}\frac{\upsilon p'}{\kappa}d\varepsilon_\theta + dp'\left[1+\frac{9}{M^2}\frac{(1-2\nu')}{(1+\nu')}\frac{\left(\sigma'_r-p'\right)}{\left(2-\left(p'_o/p'\right)^{1/\Lambda}\right)p'}\right] \tag{8a}$$

$$d\sigma'_\theta = 3\frac{(1-2\nu')}{(1+\nu')}\frac{\upsilon p'}{\kappa}d\varepsilon_\theta + dp'\left[1+\frac{9}{M^2}\frac{(1-2\nu')}{(1+\nu')}\frac{\left(\sigma'_\theta-p'\right)}{\left(2-\left(p'_o/p'\right)^{1/\Lambda}\right)p'}\right] \tag{8b}$$

$$d\sigma'_z = dp'\left[1+\frac{9}{M^2}\frac{(1-2\nu')}{(1+\nu')}\frac{\left(\sigma'_z-p'\right)}{\left(2-\left(p'_o/p'\right)^{1/\Lambda}\right)p'}\right] \tag{8c}$$

Equation 8c may be rearranged to give:

$$d\sigma'_z - dp' = d\left(\sigma'_z-p'\right) = \frac{9}{M^2}\frac{(1-2\nu')}{(1+\nu')}\frac{\left(\sigma'_z-p'\right)}{\left(2-\left(p'_o/p'\right)^{1/\Lambda}\right)}\frac{dp'}{p'} \tag{9a}$$

or

$$\frac{d\left(\sigma'_z-p'\right)}{\left(\sigma'_z-p'\right)} = \frac{9}{M^2}\frac{(1-2\nu')}{(1+\nu')}\frac{dp'}{p'\left(2-\left(p'_o/p'\right)^{1/\Lambda}\right)} \tag{9b}$$

and, finally,

$$dln\left(\sigma'_z-p'\right) = \mathrm{P}\frac{dp'}{p'\left(2-\left(p'_o/p'\right)^{1/\Lambda}\right)} \tag{9c}$$

where $\mathrm{P} = \frac{9}{M^2}\frac{(1-2\nu')}{(1+\nu')}$.

Integration of Eq. 9c gives (See appendix):

$$\sigma'_z = p' + \left(\sigma'_{zi}-p'_i\right)\left[\frac{2-\left(p'_o/p'\right)^{1/\Lambda}}{2-\left(p'_o/p'_i\right)^{1/\Lambda}}\left(\frac{p'_i}{p'}\right)^{1/\Lambda}\right]^{\mathrm{P}\Lambda/2} \tag{10}$$

The remaining principal effective stresses σ'_z and σ'_θ are found by introducing Eq. 10 into the expressions of the mean effective stress p' and the deviator stress q, as given by Eqs. 1a and 1b, resulting into:

$$\sigma'_r = p' - \frac{\left(\sigma'_{zi}-p'_i\right)}{2}\left[\frac{2-\left(p'_o/p'\right)^{1/\Lambda}}{2-\left(p'_o/p'_i\right)^{1/\Lambda}}\left(\frac{p'_i}{p'}\right)^{1/\Lambda}\right]^{\mathrm{P}\Lambda/2} + \tau \tag{11a}$$

and

$$\sigma'_\theta = p' - \frac{\left(\sigma'_{zi} - p'_i\right)}{2}\left[\frac{2 - \left(p'_o/p'\right)^{1/\Lambda}}{2 - \left(p'_o/p'_i\right)^{1/\Lambda}}\left(\frac{p'_i}{p'}\right)^{1/\Lambda}\right]^{P\Lambda/2} - \tau \tag{11b}$$

where the shear stress τ in the horizontal plane $(r:\theta)$ is equal to $\left(\sigma'_r - \sigma'_\theta\right)/2$ and is given by:

$$\tau = \frac{1}{2}\left\{\frac{4}{3}q^2 - 3\left(\sigma'_{zi} - p'_i\right)^2\left[\frac{2 - \left(p'_o/p'\right)^{1/\Lambda}}{2 - \left(p'_o/p'_i\right)^{1/\Lambda}}\left(\frac{p'_i}{p'}\right)^{1/\Lambda}\right]^{P\Lambda}\right\}^{1/2} \tag{12}$$

The natural shear strain γ is found by integration of the incremental shear strain $d\gamma = |d\varepsilon_r - d\varepsilon_\theta| = 2d\varepsilon_\theta$, which is determined from Eqs. 5a and 5b, that is, from

$$d\gamma = \frac{d\tau}{G'} - \frac{6\kappa\tau dp'}{\upsilon M^2 p'\left(2p' - p'_c\right)} \tag{13a}$$

or

$$d\gamma = \frac{2}{3}\frac{(1+\nu')}{(1-2\nu')}\frac{\kappa d\tau}{\upsilon p'} - \frac{6\kappa\tau dp'}{\upsilon M^2 p'\left(2p' - p'_c\right)} \tag{13b}$$

where G' is given by Eq. 6. Integration of Eq. 13b gives:

$$\gamma = \frac{2}{3}\frac{\kappa(1+\nu')}{\upsilon(1-2\nu')}\int_0^\tau \frac{d\tau}{p'} - \frac{6\kappa}{\upsilon M^2}\int_{p'_i}^{p'} \frac{\tau dp'}{p'\left(2p' - p'_c\right)} \tag{14}$$

where the hardening parameter $p'_c = p'\left(p'_o/p'_i\right)^{1/\Lambda}$ from Eq. 7. It is apparent that the shear strain γ in Eq. 14 must be evaluated numerically due to the complex nature of the expression of the shear stress τ from Eq. 12.

Computations of total radial stress and pore pressure were carried out following the same approach of Silvestri and Abou-Samra (2012). For completeness, their expressions are briefly repeated herein.

The total radial stress σ_r acting in the clay around the expanding cylindrical cavity is given by (Yu 2000; Silvestri and Abou-Samra 2012):

$$\sigma_r = \int_0^\gamma \frac{\tau d\gamma}{e^\gamma - 1} + \sigma_{ri} \tag{15a}$$

which becomes

$$\sigma_{ra} = \int_0^{\gamma_a} \frac{\tau d\gamma}{e^{\gamma} - 1} + \sigma_{ri} \tag{15b}$$

at the wall of the cavity, where σ_{ri} is the initial total radial or horizontal stress, and the natural shear strains γ and γ_a are given by:

$$\gamma = ln[\left(\frac{r'}{r}\right)^2] \tag{16a}$$

and

$$\gamma_a = ln[\left(\frac{a'}{a}\right)^2] \tag{16b}$$

at the wall of the cavity. The pore pressure is determined by subtracting the radial effective stress σ'_r given by Eq. 11a from the radial total stress σ_r given by Eq. 15a. In Eqs. 16a and 16b, (r, r') and (a, a') represent respectively, generic radial distances and cavity radii, before and after the distortion has occurred. In order to obtain the limiting radial expansion pressure at the wall of the cavity, it is convenient to use the Almansi tangential strain which is defined as (Baguelin et al. 1978):

$$\alpha = \frac{1}{2}\left(\frac{r'^2 - r^2}{r'^2}\right) \tag{17a}$$

which becomes equal to

$$\alpha_a = \frac{1}{2}\left(\frac{a'^2 - a^2}{a'^2}\right) \tag{17b}$$

at the wall of the cavity. Substitution of Eqs. 17a and 17b into Eqs. 16a and 16b gives:

$$\gamma = -ln(1 - 2\alpha) \tag{18a}$$

and

$$\gamma_a = -ln(1 - 2\alpha_a) \tag{18b}$$

which, when introduced into Eqs. 15a and 15b yield:

$$\sigma_r = \int_0^{\alpha} \frac{\tau d\alpha}{\alpha} + \sigma_{ri} \tag{19a}$$

and

$$\sigma_{ra} = \int_0^{\alpha_a} \frac{\tau d\alpha}{\alpha} + \sigma_{ri} \tag{19b}$$

at the wall of the cavity, as also obtained by Baguelin et al. (1978). As mentioned above, the Almansi tangential strain was introduced for facilitating the determination of the limiting radial expansion pressure. Indeed, consideration of the upper limit of the integral in Eq. 15b indicates that γ_a must be equal to infinity for the radial pressure to reach the limiting expansion condition. Such a calculation may involve considerable computational problems. However, because Eq. 18b shows that $\gamma_a = \infty$ is reached for $\alpha_a = 0.5$, then it becomes relatively easy to carry on the integration process in Eq. 19b up to $\alpha_a = 0.5$ without experiencing any computational difficulties. This shows the superiority of the Almansi tangential strain over the natural strain in extending the integration process to infinity. There is also an additional advantage. In effect, in several software programs involving either finite elements or finite differences, it is often assumed that critical state is reached when the cavity radius has doubled in size, that is, when $a' = 2a$ in order to avoid numerical difficulties. As this condition corresponds to $\alpha_a = 0.375$ from Eq. 17b or to $\gamma_a = 1.386$ from Eq. 18b, it is apparent that the limiting state of $\alpha_a = 0.5$ is still far away and that by setting $\alpha_a = 0.375$ can only result in approximate limiting values.

3 Application

Before discussing in detail the application of the various theoretical expressions derived previously to the benchmark case presented below, it should be mentioned that the Modified Cam Clay model is known to give reasonable results only for isotropically normally consolidated clays (See, for example, Wood 2007). If either the initial stress state or the clay fabric, or both, are anisotropic, or if the soil is overconsolidated, better models should be resorted to, for example, such as the anisotropic Modified Cam Clay model (Dafalias 1987; Dafalias et al. 2002, 2006) or the Banerjee model (Banerjee and Yousif 1986; Banerjee et al. 1988). These two models have the advantage over more sophisticated and complex models that they can account for both inherent and induced anisotropy with relatively few model parameters. It is the authors' intention to apply one of these models to the problem at hand in the near future.

However, as the principal aim of the present study was to obtain the exact solution of the principal effective stresses generated around a cylindrical cavity in Modified Cam Clay under plane strain and undrained conditions, computations were carried out assuming that the Modified Cam Clay model could also be applied to a K_o normally consolidated clay.

The theoretical relationships derived previously will be applied to the simulation of a plane strain undrained expansion of a cylindrical cavity in K_o normally consolidated remoulded Boston Blue Clay modelled as Modified Cam Clay. The properties of the clay are the following (Randolph et al. 1979): OCR = 1, $K_o = 0.55$, $\upsilon = 2.16$,

$\lambda = 0.15, \kappa = 0.03, \Lambda = 0.8$, and $M = 1.2$ for $\phi' = 30°$. The OCR is based on the vertical effective stress.

The initial stress conditions are represented for illustration purposes by: $\sigma'_{zi} = 300$ [kPa], $\sigma'_{ri} = \sigma'_{\theta i} = 165$ [kPa], $u_i = 0$, $p'_i = 210$ [kPa], $q_i = 135$ [kPa], $p'_o = 256$ [kPa], $p'_c = 270$ [kPa], and Poisson's ratio $\nu' = 0.2855$. The choice of $\nu' = 0.2855$ was made so that the value of the initial shear modulus G'_i, calculated from Eq. 6, was equal to that obtained from the data of Randolph et al. (1979), that is, $G'_i = 7570$ [kPa]. These authors assumed $G' = G'_i =$ constant in the entire expansion process. The stress parameters at critical state are $p'_f = 147.6$ [kPa], $q_f = 177.1$ [kPa].

Figure 2 compares the shear stress-shear strain curve obtained in this study with that derived by assuming G' to remain constant. Examination of two curves shows that they are similar.

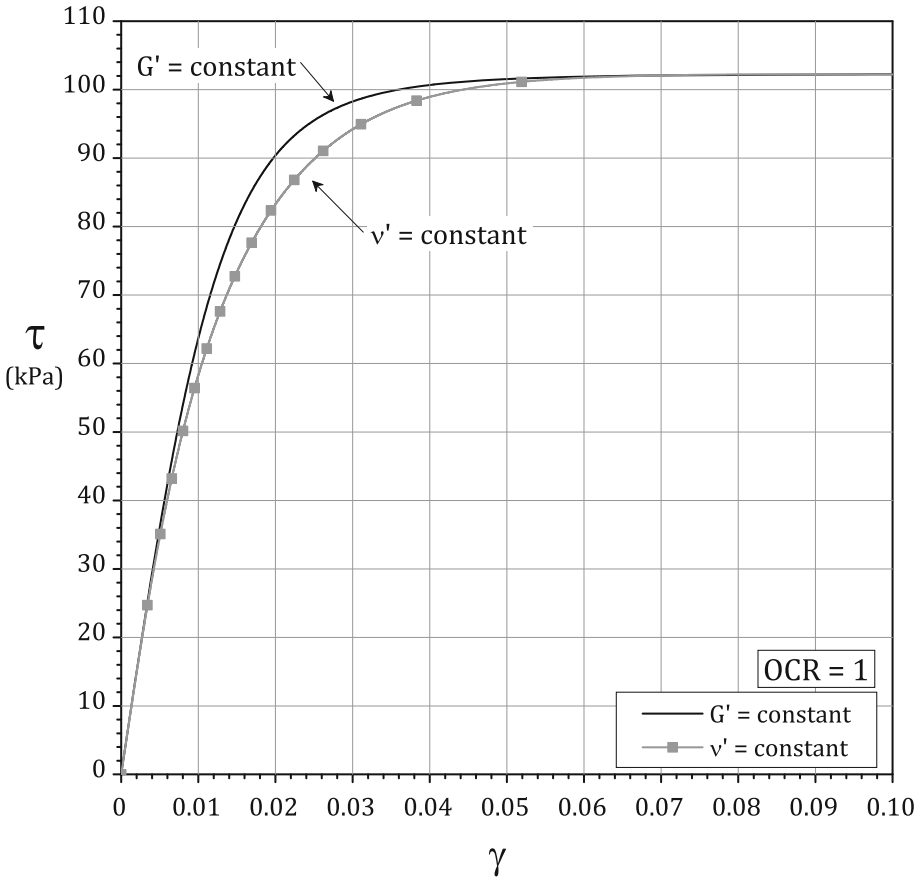

Fig. 2. Shear stress-shear strain curves

Figure 3 compares the total radial stress σ_{ra} and the excess of pore pressure u generated at the wall of the cavity as a function of the Almansi tangential strain α_a. Again, comparison between the two sets of curves indicates that the results are practically equivalent.

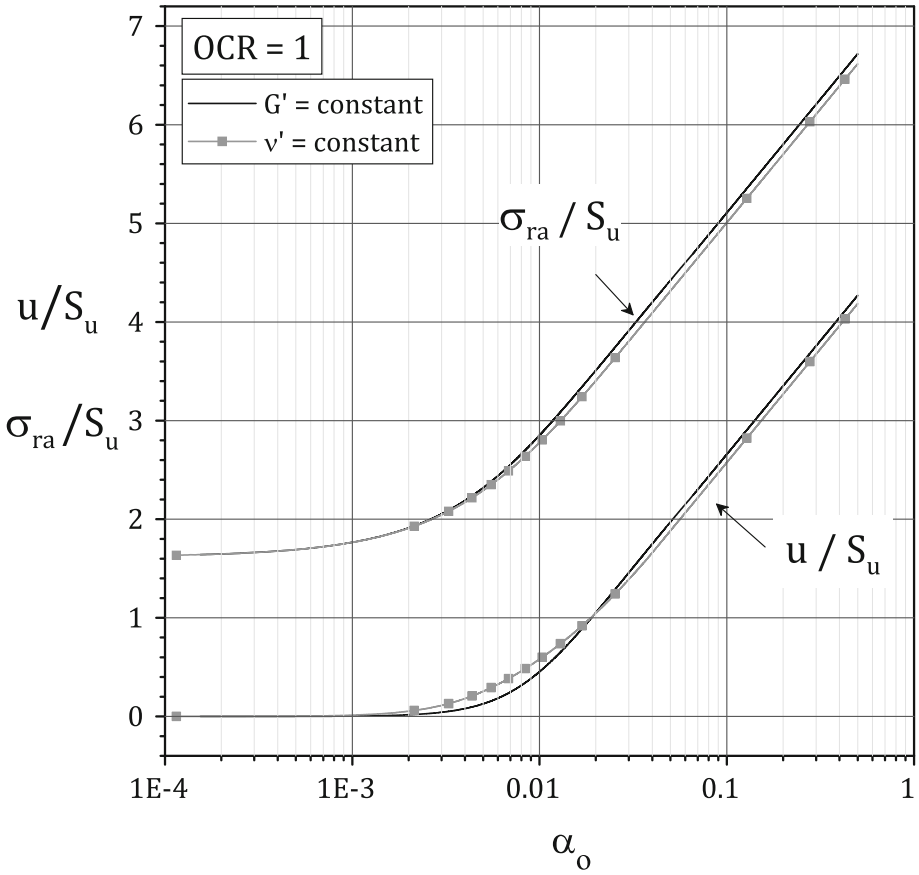

Fig. 3. Comparison of total radial stress and excess pore water pressure generated at wall of cavity as function of Almansi tangential strain α_a

Finally, Fig. 4 shows the distributions of the principal effective stresses and of the excess pore pressures around the cylindrical cavity at critical state. Once again, the two series of curves are quite similar.

Although the two sets of results presented in Figs. 2, 3 and 4 are practically equivalent, the approach followed in the present paper, by assuming Poisson's ratio ν' to remain constant during shearing, is superior to that in which the initial shearing modulus G' remains constant, because the present solution allows finding exact explicit expressions for the principal effective stresses.

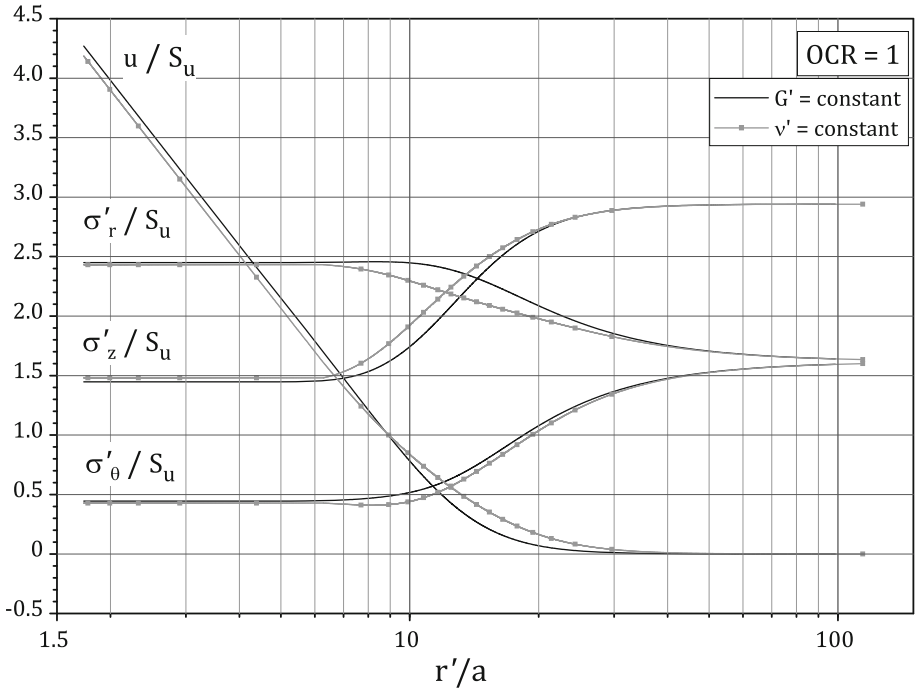

Fig. 4. Distributions of principal effective stresses and excess pore water pressures around cylindrical cavity at critical state

4 Conclusions

On the basis of the results reported in this paper, the following main conclusions are drawn:

1. The assumption of constant Poisson's ratio allows obtaining explicit expressions for the principal effective stresses generated around an expanding cylindrical cavity in Modified Cam Clay.
2. The theoretical relationships are applied to the simulation of an expanding cylindrical cavity in K_o normally consolidated remoulded Boston Blue Clay. The results, which are compared with those obtained by assuming that the shear modulus G' remains constant during the expansion, show that the two approaches are quite similar.

Acknowledgements. The author expresses his gratitude to the Natural Sciences and Engineering Research Council of Canada for the financial support received in this study.

Appendix: Derivation of Eq. 10

The integral in Eq. 9c reads

$$ln\left(\frac{\sigma'_z - p'}{\sigma'_{zi} - p'_i}\right) = \mathrm{P}\int_{p'_i}^{p'} \frac{dp'}{p'\left(2 - \left(p'_o/p'\right)^{1/\Lambda}\right)} \tag{A1}$$

where $\mathrm{P} = \frac{9}{M^2}\frac{(1-2\nu')}{(1+\nu')}$.

By letting $y = \left(p'_o/p'\right)^{1/\Lambda}$, then $p' = p'_o y^{-\Lambda}$ and $dp' = p'_o(-\Lambda)y^{-\Lambda-1}dy$, and the integral in Eq. A1 becomes

$$\mathrm{I} = -\mathrm{P}\Lambda\int_{\left(p'_o/p'_i\right)^{1/\Lambda}}^{\left(p'_o/p'\right)^{1/\Lambda}} \frac{dy}{y(2-y)} = \mathrm{P}\Lambda\int_{\left(p'_o/p'_i\right)^{1/\Lambda}}^{\left(p'_o/p'\right)^{1/\Lambda}} \frac{dy}{(y^2-2y)} \tag{A2}$$

Integration of Eq. A2 yields:

$$\mathrm{I} = -\frac{\mathrm{P}\Lambda}{2} ln\left(\frac{y}{y-2}\right)\Bigg|_{y_i}^{y} \tag{A3}$$

or

$$\mathrm{I} = -\frac{\mathrm{P}\Lambda}{2} ln\left[\left(\frac{y}{y_i}\right)\left(\frac{y_i-2}{y-2}\right)\right] = \frac{\mathrm{P}\Lambda}{2} ln\left[\left(\frac{y_i}{y}\right)\left(\frac{y-2}{y_i-2}\right)\right] \tag{A4}$$

where $y = \left(p'_o/p'\right)^{1/\Lambda}$ and $y_i = \left(p'_o/p'_i\right)^{1/\Lambda}$. As a result, Eq. A4 becomes:

$$\mathrm{I} = \frac{\mathrm{P}\Lambda}{2} ln\left\{\left[\frac{\left(p'_o/p'\right)^{1/\Lambda}-2}{\left(p'_o/p'_i\right)^{1/\Lambda}-2}\right]\left(\frac{p'_i}{p}\right)^{1/\Lambda}\right\} \tag{A5}$$

Combining Eq. A5 with Eq. A1 yields:

$$\sigma'_z - p' = \left(\sigma'_{zi} - p'_i\right)\left\{\left[\frac{\left(p'_o/p'\right)^{1/\Lambda}-2}{\left(p'_o/p'_i\right)^{1/\Lambda}-2}\right]\left(\frac{p'_i}{p'}\right)^{1/\Lambda}\right\}^{\frac{\mathrm{P}\Lambda}{2}} \tag{A6}$$

which, when rearranged, gives:

$$\sigma'_z = p' + \left(\sigma'_{zi} - p'_i\right)\left\{\left[\frac{2-\left(p'_o/p'\right)^{1/\Lambda}}{2-\left(p'_o/p'_i\right)^{1/\Lambda}}\right]\left(\frac{p'_i}{p'}\right)^{1/\Lambda}\right\}^{\frac{\mathrm{P}\Lambda}{2}} \tag{A7}$$

Eq. A7 is Eq. 10 in the main text of the paper.

References

Baguelin, F., Jézéquel, J.F., Shields, D.H.: The Pressuremeter and Foundation Engineering. Trans Tech Publications, Clausthal (1978)

Banerjee, P.K., Yousif, N.B.: A plasticity model for the mechanical behaviour of anisotropically consolidated clay. Int. J. Numer. Anal. Meth. Geomech. **10**(5), 521–541 (1986)

Banerjee, P.K., Kumbhojkar, A.S., Yousif, N.B.: Finite element analysis of the stability of vertical cut using an anisotropical soil model. Canad. Geotechn. J. **25**(1), 119–127 (1988)

Cao, L., Teh, C.I., Chang, M.-F.: Undrained cavity expansion in modified Cam clay I: theoretical analysis. Géotechnique **51**(4), 323–334 (2001)

Chen, S.L., Abousleiman, Y.N.: Exact undrained elasto-plastic solution for cylindrical cavity expansion in modified Cam clay. Géotechnique **62**(5), 447–456 (2012)

Dafalias, Y.F.: An anisotropic critical state clay plasticity model. In: Proceedings of the Second International Conference on Constitutive Laws for Engineering Materials. Theory and Applications, Tucson, Arizona, vol. 1, pp. 513–521. Elsevier, 5–8 January 1987

Dafalias, Y.F., Manzari, M.T., Akaishi, M.: A simple anisotropic clay plasticity model. Mech. Res. Commun. **29**(4), 241–245 (2002)

Dafalias, Y.F., Manzari, M.T., Papadimitriou, A.G.: SANICLAY: simple anisotropic clay plasticity model. Int. J. Numer. Anal. Meth. Geomech. **30**(12), 1231–1257 (2006)

Gens, A., Potts, D.: Critical state models in computational geomechanics. Eng. Comput. **5**, 178–197 (1988)

Monnet, J.: Numerical validation of an elasto-plastic formulation of the conventional limit pressure measured with the pressuremeter test in cohesive soil. ASCE J. Geotech. Geoenviron. Eng. **133**(9), 1119–1127 (2007)

Randolph, M.F., Carter, J.P., Wroth, C.P.: Driven piles in clay-the effect of installation and subsequent consolidation. Géotechnique **24**(4), 361–393 (1979)

Silvestri, V., Abou-Samra, G.: Analytical solution for undrained plane strain expansion of a cavity in modified Cam clay. Geomech. Eng. **4**(1), 19–37 (2012)

Yu, H.S.: Plasticity and Geotechnics. Springer, New York (2006)

Yu, H.S.: Cavity Expansion Methods in Geomechanics. Kluwer Academic Publishers, Dordrecht (2000)

Wood, D.M.: Soil Behaviour and Critical State Soil Mechanics. Cambridge University Press, Cambridge (2007)

Zytynski, M., Randolph, M.F., Nova, R., Wroth, C.P.: On modelling the unloading-reloading behaviour of soils. Int. J. Numer. Anal. Meth. Geomech. **2**(1), 87–93 (1978)